J Mater Sci (2017) 52:804–814

Varied hydrogen evolution reaction properties of nickel phosphide nanoparticles with different compositions in acidic and alkaline conditions

Lei Wan[1,2], Jinfeng Zhang[1], Yaqiong Chen[2], Cheng Zhong[1], Wenbin Hu[1,2], and Yida Deng[1,*]

[1] *Key Laboratory of Advanced Ceramics and Machining Technology (Ministry of Education), and Tianjin Key Laboratory of Composite and Functional Materials, Tianjin University, Tianjin 300072, People's Republic of China*

[2] *State Key Laboratory of Metal Matrix Composites, Shanghai Jiao Tong University, Shanghai 200240, People's Republic of China*

Received: 9 June 2016
Accepted: 6 September 2016
Published online: 14 September 2016

ABSTRACT

This paper introduces HER activity of a string of Ni–P nanoparticles. The hydrogen evolution reaction (HER) activity of different Ni–P nanoparticles hinges on elemental ratios of nickel to phosphorus and nickel phosphide phases through annealing processes, which lead to utter diverse HER performances in H_2SO_4 and NaOH. The sample annealed under 350 °C by 4 h, mainly comprised by Ni_3P and $Ni_{12}P_5$, shows overpotential of 333 mV to achieve 100 mA·cm^{-2} (η_{100} = 333 mV) current density in acidic condition, whereas in alkaline condition, the non-heat-treated sample, mainly formed by $Ni_{12}P_5$ and Ni_2P, shows the best HER performance. Ni–P nanoparticles have also displayed distinguished durability in both H_2SO_4 and NaOH. The superior HER activity and durability are supported by a series of characterizations and stem from Ni–P nanoparticles' nature, including their morphology, good ensemble effect between nickel and phosphorus, and anti-corrosive quality.

Introduction

Research and development of clean and renewable energy has been an urgent demand, and among renewables, hydrogen is considered as a promising one [1–3]. Apart from its potential role as the alternative for fossil fuels, it has long been the raw materials for petroleum refining and synthetic ammonia industry [1]. Electrochemical methods, including electrolysis or photoelectrochemical water splitting, facilitated by other renewables are regarded as hopeful means to generate hydrogen in large scale [1–4]. These methods are usually in need of an effective catalyst, and by far the most high-performance one has been platinum. Unfortunately, hobbled by platinum's inherent scarcity in the earth's crust, someday it must be replaced by a more cost-effective one.

Transitional metal sulfides and phosphides are the main focuses of academics' efforts to prepare ideal substitutes of platinum. These sulfides and

Address correspondence to E-mail: yida.deng@tju.edu.cn

DOI 10.1007/s10853-016-0377-7

phosphides have largely improved instable problems of the Ni-based alloys amid acidic solution [5, 6], and meanwhile show remarkable HER activity (though they are still inferior than platinum). MoS_2 and Ni_2P are two examples of the two groups both in theoretical calculation and detailed experiments [7–10], from which related derivatives inspired by them were frequently reported, for instance, CoP [11], Cu_3P [12], MoP [1], FeP [13], and Ni_xP_y [14]. Ni_xP_y is a "catch-all" term for a group of nickel phosphides, including Ni_2P [5, 10, 11], Ni_5P_4 [2, 15], Ni_3P [16, 17], $Ni_{12}P_5$ [15, 18], etc. The fact that nickel is comparatively more abundant than molybdenum has previously made pure nickel more often used than molybdenum [5]. This more or less leads to the popularity of related research about Ni_xP_y.

This paper introduces a series of Ni–P nanoparticles' HER activity. Although a facile reduction reaction method, which is surfactant free, does not require any expensive materials or draconian reaction conditions, and the follow-up processes [19, 20], the products, that mainly comprised $Ni_{12}P_5$, Ni_2P, and Ni_3P, of different heat treatment times have shown diverse and favorable HER activity. Inspired by the typical electroless plating technique that heat treatment will cause phase transformation of Ni–P alloys [14, 21], the as-synthesized samples would experience a series of annealing processes. Among samples of different degrees of heat treatment, the 4-h-annealed one displays the best HER activity in H_2SO_4 and the non-annealed one performs the greatest in NaOH. This phenomenon is mainly caused by different patterns of manifestation of ensemble effect between charged nickel and phosphorus, which is decided by both element ration of nickel to phosphorus and phases of nickel phosphide [2, 5, 7, 15]. Apart from the ensemble effect, the superior HER activity is also accredited by the nanoparticles' excellent dispersity and small size. Their durability after long-term electrochemical measurements, declines little, which gives them the potentiality and value of being studied further in the future.

Experimental section

Materials

Nickel sulfate ($NiSO_4$), sodium hydroxide (NaOH), acetic acid (CH_3COOH), palladium chloride ($PdCl_2$), sodium hypophosphite (NaH_2PO_2), ammonium hydroxide ($NH_3{\cdot}H_2O$), hydrochloric acid (HCl) and sulfuric acid (H_2SO_4) were all purchased from National Chemical Reagent Ltd., Shanghai, China, without any purification. The raw materials were prepared into different concentrations by deionized water (18.2 MΩ cm) prepared from a Millipore ultrapure water system.

Synthesis and subsequent processing of Ni–P nanoparticles

Synthesis of Ni–P nanoparticles comprised three steps. The first step was the preparation of α-$Ni(OH)_2$ nanowires by $NiSO_4$ and NaOH, which drew on a hydrothermal method [20]. Utilizing a facile and fast autocatalytic reduction method [19], then the as-synthesized $Ni(OH)_2$ precursors would react with NaH_2PO_2 which served as the reducing agent. The reaction process was helped by $PdCl_2$ and CH_3COOH as nucleate agent and pH regulator and generated original black Ni–P nanoparticles. In the last step, the original Ni–P nanoparticles would be soaked first in stronger $NH_3{\cdot}H_2O$ by 24 h and then in mixed acid (0.5 M H_2SO_4 and 0.5 M HCl) by 2 h. The final Ni–P nanoparticles were obtained after repeatedly being rinsed by deionized water. Before any characterizations and measurements, some of the as-prepared Ni–P nanoparticles will be annealed amid 5 % H_2/Ar atmosphere by 4 and 8 h.

Characterizations

A 204 F1 differential scan calorimeter was employed to get the output of differential scanning calorimetry and thermogravimetric analysis (DSC/TGA) plots. The testing temperature ranged from 25 °C (298 K) to 500 °C, and the heating rate was 10 °C min^{-1}, aiming to sketchily determine the heat treatment temperature. X-ray diffraction (XRD) was performed by D/max-IIIA X-ray diffractometer with Cu-Kα radiation (λ = 1.54056 Å). A Kratos AXIS ultra X-ray photoelectron spectroscope (XPS) was used to get XPS data, with its incident radiation being 150 W KR X-rays. TEM images of Ni–P nanoparticles were collected by a JEM-2100F transmission electron microscope. The molar ratio of Ni and P was accurately pinned down by a iCAP6300 inductively coupled plasma-optical emission spectrometer (ICP).

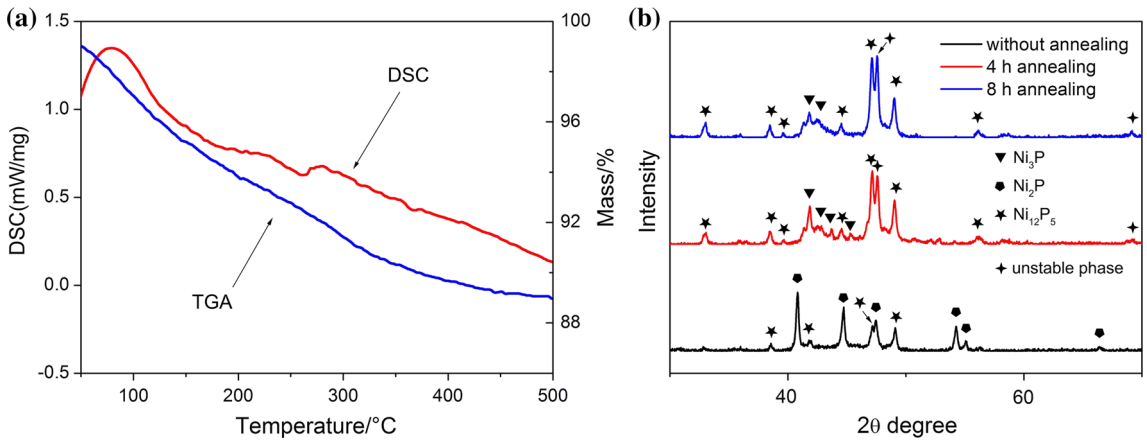

Figure 1 **a** DSC/TGA curves of the Ni–P nanoparticles. **b** XRD patterns of Ni–P nanoparticles heat treated by different times.

Electrochemical measurements

Ni–P nanoparticles of different heat-treated times, mixed with ethanol and experienced ultrasonication by over 30 min, were evenly dropped on 5-mm-diameter T-shaped glass carbon electrodes (0.6 mg·cm^{-1} as loading weight) as working electrodes. Shortly after the well-dispersed ink dried out, the electrodes were sealed by Nafion solution (2 wt%, 100 μL). The electrolyte was either 0.5 M H_2SO_4 or 1 M NaOH which was purged by high-purity N_2 ahead of any electrochemical measurements to make the solution free from oxygen. Aside from the working electrodes, a platinum electrode served as the counter electrode and a saturated Ag/AgCl electrode (SSCE) or a saturated Hg/Hg_2Cl_2 (SCE) as the reference electrodes.

All of the electrochemical measurements were carried out by a electrochemical workstation (CHI 660E) in a typical three-electrode system without iR compensation. Linear sweep voltammetry (LSV) was performed to measure HER activity, with its scanning voltage ranging from −0.15 to −0.65 V in H_2SO_4 condition and −1.05 to −1.6 V in NaOH condition. Durability of the electrodes was observed by cyclic voltammetry (CV) and the potentiostatic experiment. The Nyquist plots were obtained from the electrochemical impedance spectroscopy (EIS), with 0.1–10^5 Hz as the measuring frequency at different overpotentials. Potentials presented in this paper were transformed into reversible hydrogen electrode (RHE): E(RHE) = E (SSCE) + (0.197 + 0.059 pH) or E(SCE) + (0.242 + 0.059 pH).

Results and discussion

Characterizations

Figure 1a illustrates DSC and TGA curves of the as-prepared Ni–P nanoparticles. The TGA curve does not show any particular trend. It declines gradually with the increase of the given temperature and after 400 °C, the decreasing trend starts to level off. The DSC curve, by contrast, shows an exothermic peak around 270 °C or so. When it comes to deciding of the heat treatment process, the temperature should not be either too high or too low. In a comparatively low temperature, the recrystallization process would be fairly slow, which is not a favorable situation. On the contrary, an exceedingly high temperature—for instance, 500 °C—will give rise to severe agglomeration of the nanoparticles, making it hard to disperse uniformly with ethanol and finally lowering HER activity. In view of the above-mentioned factors, 350 °C was chosen as the annealing temperature. The Ni–P nanoparticles were divided into three independent samples: the first one would not be annealed; the second one was heat treated by 4 and 8 h for the last one.

X-ray diffraction patterns of samples heat treated by different hours are shown in Fig. 1b. The non-annealed sample consists of a combination of $Ni_{12}P_5$ (PDF 03-0953) and Ni_2P (PDF 22-1190) phases. The 4-h-annealed sample, by contrast, rules out all existed Ni_2P facets and brings in Ni_3P phase which corresponds to PDF 34-0501. Some metastable phases are also introduced to the 4 and 8-h XRD patterns. The 8-h XRD pattern is nigh-identical to the 4-h-annealed

counterpart. Generally, the final heat treatment product of nickel phosphide prepared by NaH_2PO_2 is Ni_3P [14, 21, 22] and this partly explains why Ni_3P emerges after the annealing process. On the other hand, the 8-h heat-treated sample is still dominated by $Ni_{12}P_5$ facets, which can be accredited by several causes. One apparent reason is the not adequate high annealing temperature. As a result, energy required to activate and accelerate re-crystallization and phase transformation is far from adequacy [16]. Furthermore, the result of ICP in Table 1—an accurate method to ascertain the elemental ratio—shows nickel accounting for 63.3 % and *P* representing 15.2 %, which means that the molar ratio between Ni and P is 2.20, a value between Ni_2P (2:1) and $Ni_{12}P_5$ (2.4:1). This ratio is more close to $Ni_{12}P_5$ rather than Ni_3P. While Ni_2P phase is not stable in high temperature [2], the final product cannot be fully converted into Ni_3P phase because of the mismatch of the elemental ratio. Outcomes of after-annealed samples are analogous with the non-annealed one, except for a little increase of phosphorus content with the extension of annealing duration. Therefore, after annealing process, the remaining phases are comparatively stable $Ni_{12}P_5$ and Ni_3P phases.

Table 1 ICP results of different Ni–P nanoparticle samples

Annealing time	Non-annealed	4 h	8 h
Ni (wt%)	63.3 %	63.53 %	62.87 %
P (wt%)	15.2 %	15.78 %	16.11 %
n (Ni):n(P)	2.20	2.16	2.06

XPS Spectra in Fig. 2 give a further insight into the composition of the as-synthesized nanoparticles. In Fig. 2a, two small peaks at around 852.7 and 869.5 eV prove to be $Ni^{\delta+}$ in Ni $2p_{3/2}$ and $2p_{1/2}$ energy levels, respectively, namely the one making up Ni_xP_y [15, 23]. The values of 852.7 and 869.5 eV are just sandwiched between those values corresponding to Ni_2P and $Ni_{12}P_5$ [15], which are probably contributed by Ni_2P and $Ni_{12}P_5$. Similarly, two comparatively peaks 856.5 and 874.4 eV are attributable to oxidized Ni species of Ni $2p_{3/2}$ and $2p_{1/2}$ energy levels, respectively. The left two peaks match with $Ni^{\delta+}$ satellite peaks [24]. As for phosphorus XPS spectra, two peaks sited at 133.7 and 129.5 eV can be accredited to oxidized *P* species and the one(P^-) in Ni_xP_y [23]. Compared to the energy level 130.2 eV of elemental phosphorus, the binding energy of 129.5 is much smaller, indicating the samples' negative charge($P^{\delta-}$) [25, 26]. This P^- is actually coupled with $Ni^{\delta+}$ in Ni–P nanoparticles. XPS spectra for 4- and 8-h-annealed samples show similar traits of charged Ni and P in Fig. S1. On the face of it, the oxidized peaks in both Ni and P may suggest an overwhelming amount of oxide rather than the Ni_xP_y; however, this is just partially correct. What the XPS gives is the surface physical traits of Ni–P alloys. Chemical components between the surface and the inner site of the samples surely bear some differences. In the process of synthesis or dehydration, the surface is prone to be oxidized into oxidation state. Moreover, XRD patterns in Fig. 2b show no signal corresponding to any oxide, demonstrating that the system is mainly comprised by Ni_xP_y.

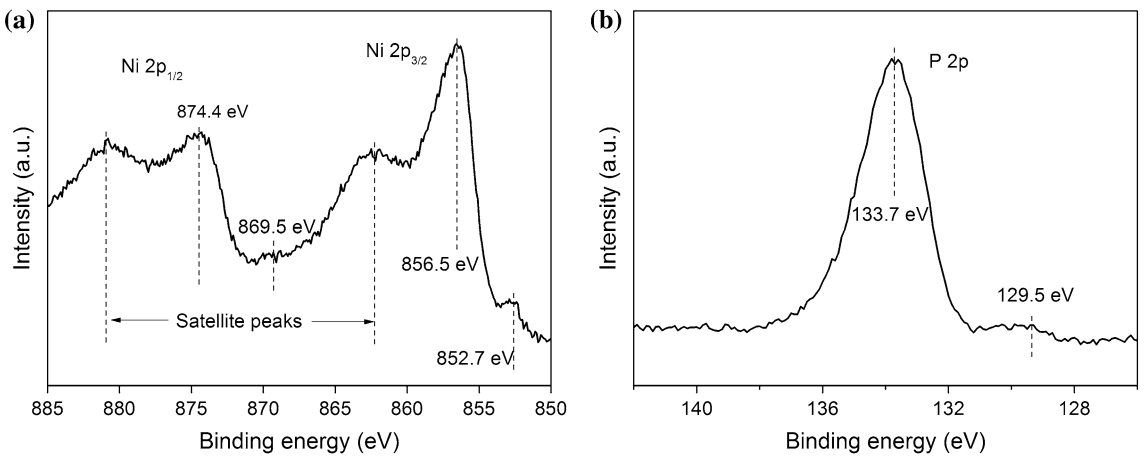

Figure 2 XPS spectra: **a** nickel, **b** phosphorus.

As shown in Fig. 3, heat treatment process does not seem to bear on nanoparticles' surface morphology. In Fig. 3a, the non-annealed sample shows some nanospheres which are well distributed in the view. The 4-h (in Fig. 3b) and 8-h (in Fig. 3c) annealed samples share a similar morphology, which implies heat treatment's limited influence on the nanoparticles' morphology. Nanoparticles in all three pictures, despite good dispersity, agglomerate more or less with one another. Nevertheless, considering the fact that the nanospheres are prepared through a surfactant-free method, this result is acceptable and acknowledged. Observed in higher resolution, as shown in Figs. 3d–f, the nanoparticles are roughly rounded, with diameter ranging from 40 to 80 nm. Again, the long-time heat treatment process has played little role to the size of the nanoparticles. As the 8-h heat-treated particles in Fig. 3f are almost the same as those in Fig. 3e (non-heat-treated one). In XRD patterns, as shown in Fig. 1b, different phases bearing various phases have been illustrated; therefore, in Fig. S2 and S3, this also leads to disorders of selected area electron diffraction and lattice fringes in high-resolution TEM images, because what make these samples vary from different phases (including the amorphous and metastable) and crystal faces.

Electrochemical analyses

Figure 4a illustrates typical polarization curves (exported by the LSV test) tested in acidic condition. HER varies in terms of different annealing lengths of time. The non-annealed sample shows comparative lower HER than its already-annealed counterparts, which needs 425 mV overpotential to reach -100 mA·cm^{-1} current density ($\eta_{100} = 425$ mV). The 4-h sample displays the lowest η_{100}, with only 362 mV, a little smaller than its 8-h-annealed equivalent (378 mV). These two figures are favorable and comparable with another already-reported Ni–P nanoparticles after taking their loadings into accounts [15, 18, 27, 28]. Another important indicator of

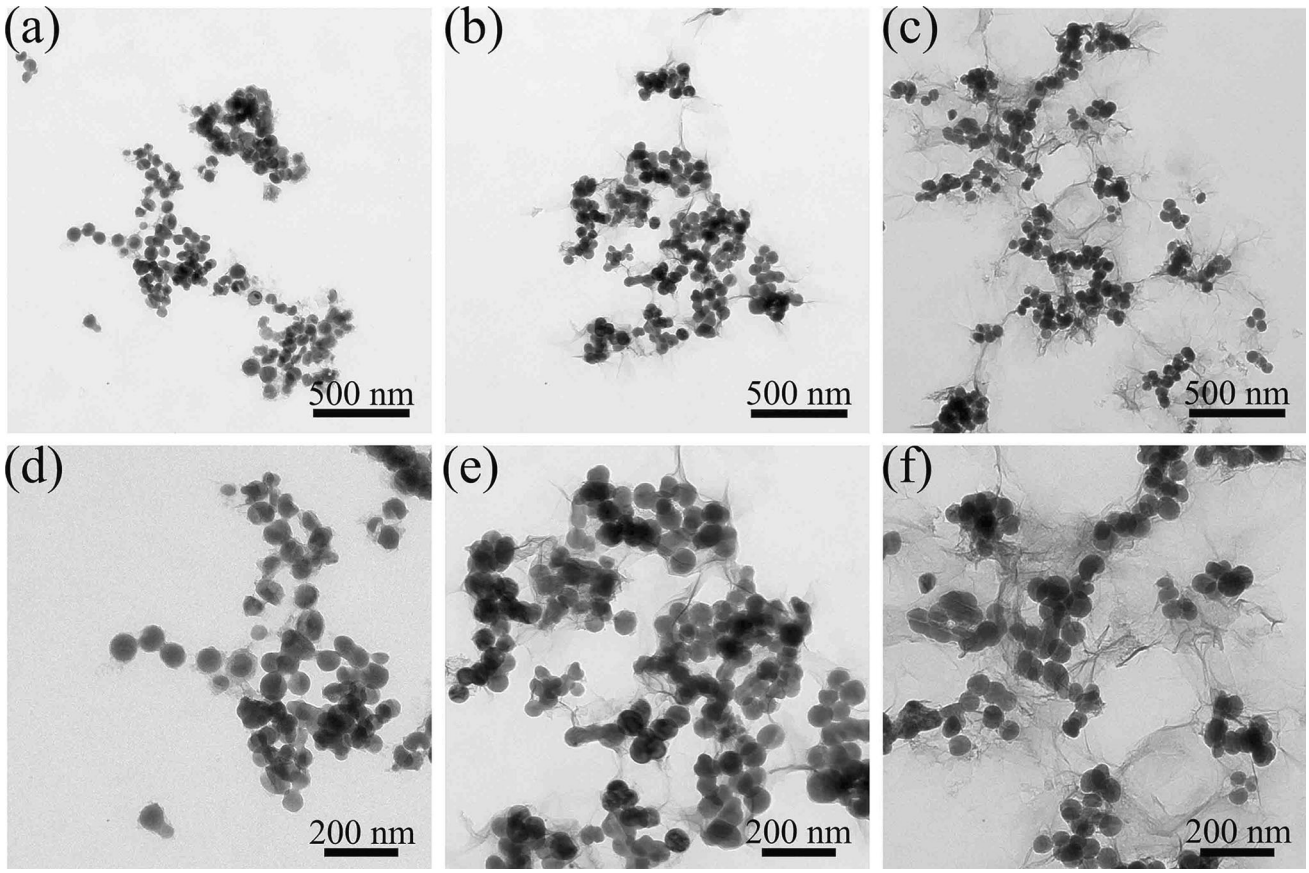

Figure 3 TEM images of Ni–P nanoparticles: **a** non-annealed sample, **b** 4-h-annealed sample, **c** 8-h-annealed sample, **d** non-annealed sample in higher resolution, **e** 4-h-annealed sample in higher resolution, **f** 8-h-annealed sample in higher resolution.

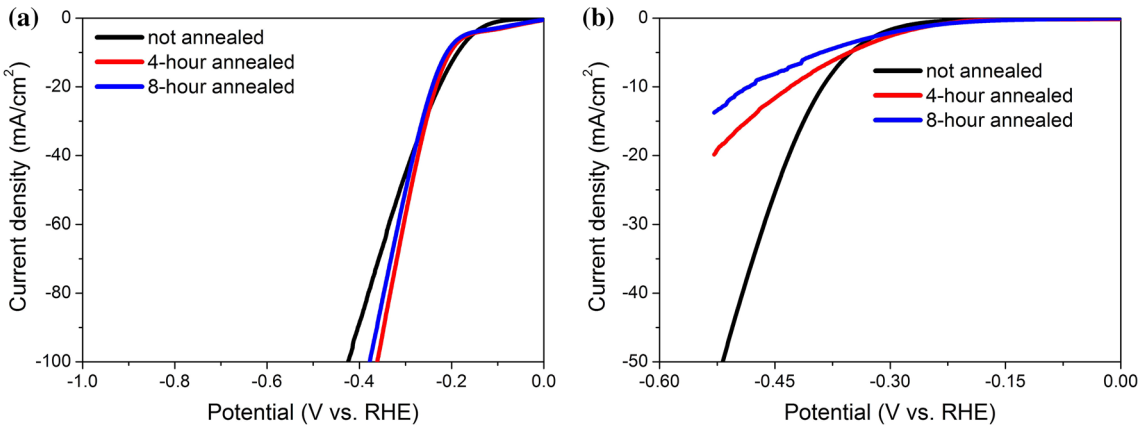

Figure 4 Polarization curves of Ni–P nanoparticle annealed by different times: **a** in 0.5M H_2SO_4, **b** in 0.5 M NaOH.

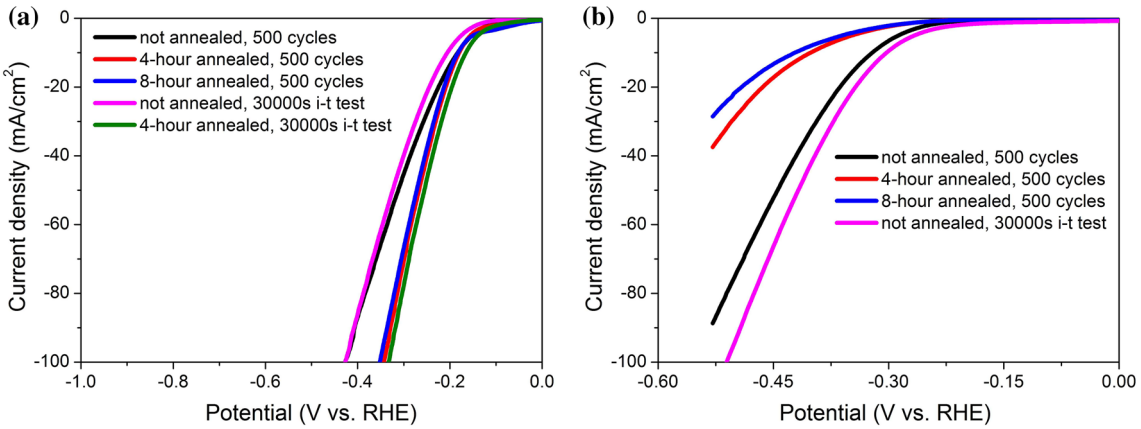

Figure 5 LSV curves after durability tests: **a** in H_2SO_4, **b** in NaOH.

nanoparticles' HER activity is η_2, generally considered as the onset potential [29, 30]. To reach -2 mA·cm^{-1}, the 4-h-annealed sample again ranks the first, at 57 mV. The corresponding values for the non-heat-treated sample and 8-h-annealed sample are 124 and 67 mV, respectively. It is also worth mentioning the 4-h-annealed sample's η_{10}—which is significant value and generally considered as ~10 % solar photoelectrical conversion efficiency [2, 31]—being 204 mV. As to the polarization curves measured in NaOH, things are quite different. While it is not strange to see that HER activity in NaOH is inferior than that in H_2SO_4, it is the non-heat-treated sample demonstrates the best performance, which requires -518 mV to reach -50 mA·cm^{-1}. The heat-treated samples, by contrast, show poor HER property. The 4-h-annealed one, again, has a better HER activity than the 8-h-annealed one, but both of them do not have more applicable values for their poor performances.

High durability in electrolyte, especially in acidic condition, is a crucial criterion for a qualified HER catalyst. After getting initial insight of HER property of samples annealed by different times, a series of durability measurements were carried out. First was the 500 cycles of CV test, which worked under the same scan voltage compared with LSV test, and then a long-term (30000 s) potentiostatic experiment was performed. The applied overpotentials to different samples were chosen according to sample's original HER activity.

After CV tests, as shown in Fig. 5a, samples tested in H_2SO_4 remain in their high HER catalytic activities. The non-annealed sample's η_{100} is 428 mV, just a little bit higher than its original activity. Corresponding η_{100} of the 4- and 8-h heat-treated samples even show a substantial decrease to 344 mV and 353 mV, respectively. The drops of overpotentials that correspond to an appointed current density are more significant in alkaline condition (in Fig. 5b). η_{50} of the non-annealed sample 445 mV has a leapfrog

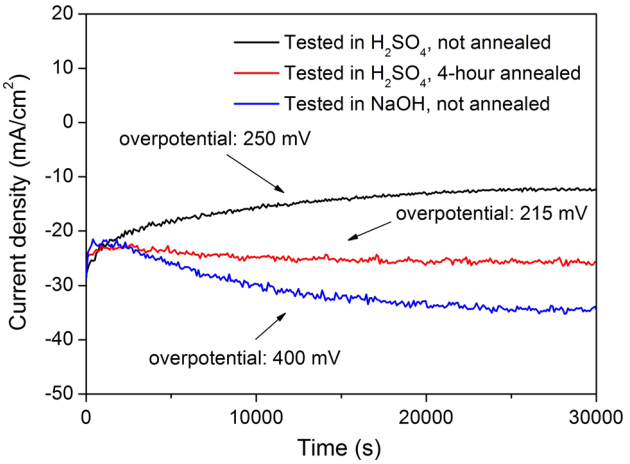

Figure 6 Time-dependent current density drawn from the potentiostatic experiment.

compared to its initial value 518 mV. Accordingly, the 4- and 8-h-annealed samples show similar trends. In regard to i–t current density curves, in acidic condition, two typical non-annealed and 4-h-annealed samples in Fig. 6 display utterly different tendencies. Starting at -28 mA·cm^{-1} under -250 mV, the non-annealed sample's current density has experienced consecutive decline until the end of the duration, to only -12.3 mA·cm^{-1}. In comparison, the 4-h treated sample under overpotential of 215 mV just witnesses marginal change in terms of current density, from -26.5 to -25.6 mA·cm^{-1}. The high durability of the 4-h-annealed sample has also been proved by its polarization curve in Fig. 5a which is almost the same to its original state. This time, η_{100} once again shows a fractional decrease to 333 mV. The same LSV test does prove the decline of the non-annealed sample's current density which matches to overpotential of 215 mV (in Fig. 5a). There exists a patent discrepancy between the black and the purple curve, but after heading to a more negative potential, the gap just narrows to a minimum difference (the black and the purple lines almost overlap with one another at this time). The i–t current density curve of non-annealed sample measured in NaOH shows an interesting trend. Under 400 mV overpotential, it first rapidly drops to -21.6 mA·cm^{-1} after 1000 s from -28.6 mA·cm^{-1} and, subsequently, commences to recapture the "loss." After 30000 s, the current density reaches -34.7 mA·cm^{-1}. Then, its η_{50} of polarization curve, as shown in Fig. 5b, comes to 418 mV, 27 mV lower than its before-CV figure, and its η_{100} is 511 mV, a value lower than η_{50} of its before-durability-test state (511 mV). HER activity of 4- and 8-h-annealed samples in NaOH, though, also make some increase, despite their still poor performances.

Through the durability tests, it can be concluded that in 0.5 M H_2SO_4, the 4-h heat-treated sample, that comprised $Ni_{12}P_5$, Ni_3P, and metastable phases, has a better acid-resisting property than the non-heat-treated one, which comprised $Ni_{12}P_5$ and Ni_2P, for its stable output current density under potentiostatic experiment. Actually, under the same designated overpotential, output current density in the polarization curve outperforms the one tested in the potentiostatic experiment. When operating potentiostatic experiment, the periodical formation and escape of air bubbles attached to the working electrode surface is the main reason for this phenomenon [32, 33]. The dramatic decline of HER activity in the initial stage (1000 s or so) in three samples is just the moment when the bubble formed. Additionally, the abnormal rising HER activity observed in both NaOH and H_2SO_4 is attributed to the process of removing the oxide from the electrode surface [32]. The XPS spectra in Fig. 2 and Fig. S1 have suggested the possibility of some amounts of oxide on the Ni–P particles' surface. The oxide will surely hinder the performance of samples' HER performance. This impediment to the HER activity is more obvious in NaOH. As oxide's acid resistance in NaOH is far better than that in H_2SO_4, the thin oxide is expected to be dissolved by H_2SO_4 as soon as possible, thus exerting little influence in terms of the HER property. When the potentiostatic experiment has completed, η_{100} of the 4-h-annealed sample tested in H_2SO_4 goes down to 333 mV from 362 mV, approximately 10 % promotion, whereas the η_{50} in NaOH jumped to 418 mV, 100 mV increase from 518 mV.

Summarized from the LSV test and the follow-up stability tests, the Ni–P nanoparticles' good HER activity can be expounded by several causes. (1) The particles' nano-scaled size, compared to bulk materials, is one important factor. The smaller the particle's size the larger the overall surface of the system, implying more active sites to trigger the catalytic reaction. (2) Additionally, the nanoparticles' superior dispersity also makes the number of would-be exposed active sites as many as possible. (3) More importantly, the HER activity is also due to the catalytic nature of nickel phosphide. Transition metal phosphides, like CoP [11], Cu_3P [12], FeP [13], MoP [34], as well as Ni_2P [5], all display superior HER

catalytic property, largely attributable to a positive charged center $M^{\delta+}$ (M = transition metals) and a negative-charged center $P^{\delta-}$ [7]. The ensemble effect between $P^{\delta-}$ and $M^{\delta+}$ is similar to [NiFe] hydrogenase, in which one part serves as hydride acceptor and the other as proton acceptor. This effect can extrapolate to other types of Ni_xP_y [15, 18], including Ni_5P_4, $Ni_{12}P_5$, and Ni_3P. In the XPS spectra (in Fig. 2), the charged $Ni^{\delta+}$ and $P^{\delta-}$ just match with this theory, which greatly promotes HER through electrochemical desorption. (4) The Ni–P nanoparticles show excellent corrosion resistance property, especially in H_2SO_4. And the annealed sample performs better in H_2SO_4 than its non-annealed counterpart, under the background of few changes of morphology or element ratio (because the heat treatment will not cause a large shift of element molar ratio at all [17]); a combination of Ni_3P, $Ni_{12}P_5$, and metastable phases may have better acid-resistance property than the non-annealed one formed by $Ni_{12}P_5$ and Ni_2P.

In NaOH and H_2SO_4, however, HER activity of different samples does not show the same trend. The non-heat-treated sample has the lowest η_{100} in NaOH and meanwhile the highest in H_2SO_4 among the three samples, which once perplexed the authors at first time. Other than a system composed by a pure phase, the Ni–P nanoparticles in one sample presented in this work mainly consist of more than one kind of Ni–P phase, like $Ni_{12}P_5$, Ni_3P, Ni_2P and some metastable transitional phases due to the annealing process [14, 16]. The combination of two or three of them will not harm the overall HER catalytic activity, since different Ni_xP_y phases will play their role independently. After the annealing process, the Ni_2P disappears because of its instability under high-temperature atmosphere, Ni_3P arises and the already-existed $Ni_{12}P_5$ changes accordingly in regard to its chiefly exposed facets, which is seen in Fig. 1b. Liu and his colleagues suggest that a higher phosphorus content leading to electron tranfer from nickel to phosphorus plays an important part in deciding overall HER activity of Ni_xP_y nanoparticles [15]. But In this occasion, an absolute conclusion cannot be made qualitatively because a few variables can influence the overall HER catalytic activity. However, it seems that non-heat-treated one, that comprised $Ni_{12}P_5$ and Ni_2P, has a slightly inferior HER activity in H_2SO_4 but performs much better in NaOH. On the other hand, the 4-h-annealed sample's HER activity in NaOH can almost be neglected. In addition, synergic effect can also happen between different phases of Ni_xP_y, which may have an impact on HER performance as well [35]. To further explain this interesting result, more works still need to be done about this.

Drawing on polarization curves in both H_2SO_4 and NaOH and in order to get more insight of the HER activity, kinetic behavior of some typical samples was analyzed by Tafel plots, which are shown in Fig. 7. All of them have shown a typical Tafelian behavior, whose equation is given by

$$\eta = b \log j + a \quad (1)$$

In this equation, η, j, b, and a are the overpotential, the corresponding current density, the Tafel slope, and the intercept, respectively. Among these parameters, the Tafel slope serves as the most important one that determines the overpotential to increment of output current density. Therefore, the smaller the Tafel slope, generally the less needed overpotential and the better HER activity.

In H_2SO_4, the non-annealed sample's Tafel slope proves to be 104 $mV \cdot dec^{-1}$, a little larger than its 4-h-annealed counterpart. Similarly, under alkaline condition, the non-annealed sample's Tafel slope is 125 $mV \cdot dec^{-1}$, while after 30000 s of potentiostatic experiment, the Tafel slope drops to 121 $mV \cdot dec^{-1}$. These results are well matched with those presented in previous electrochemical characterizations. These two figures of Tafel slope suggest that the reaction is determined by both Heyrovsky and Volmer reactions, while in NaOH, it is the Volmer reaction that

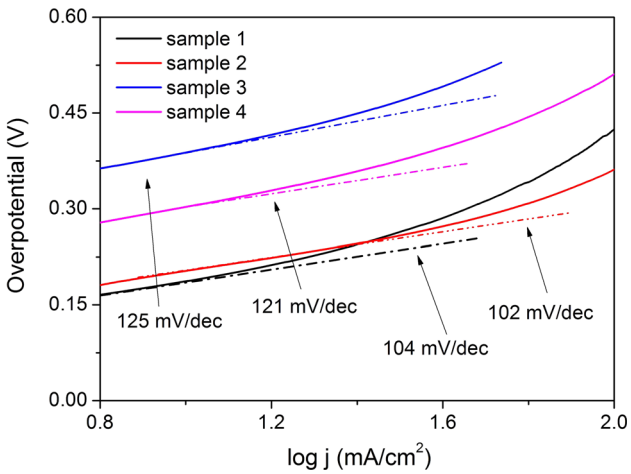

Figure 7 Tafel plots of Ni–P nanoparticles: **a** non-annealed sample, tested in H_2SO_4, **b** 4-h-annealed sample, tested in H_2SO_4, **c** non-annealed sample, tested in NaOH, **d** non-annealed sample, after 30000 s potentiostatic experiment, tested in NaOH.

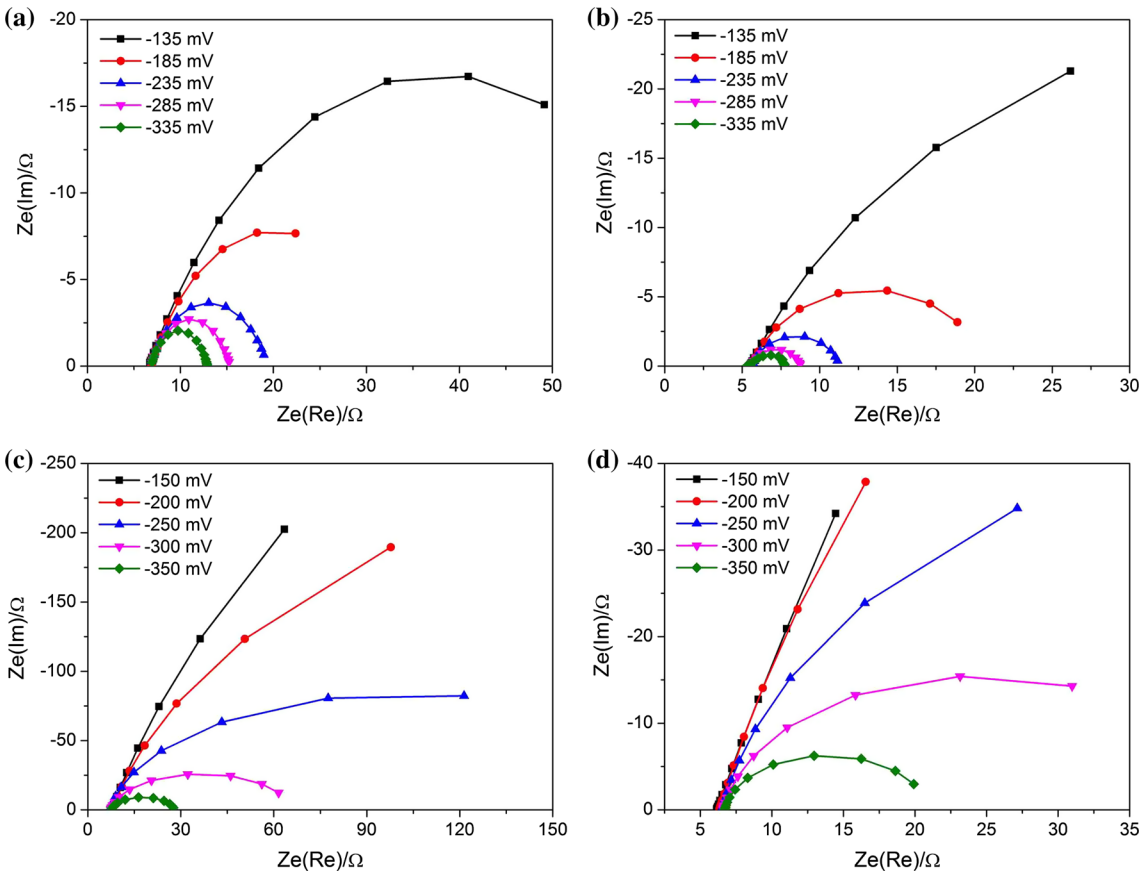

Figure 8 Nyquist plots of Ni–P nanoparticles under different overpotentials: **a** non-annealed sample, tested in H_2SO_4, **b** 4-h-annealed sample, tested in H_2SO_4, **c** non-annealed sample, tested in NaOH, **d** non-annealed sample, after 30000 s potentiostatic experiment, tested in NaOH.

counts as the rate-determining step for the Tafel slopes of 125 and 121 mV·dec^{-1}.

The Nyquist plots shown in Fig. 8 obtained by EIS experiments are also in line with the above-mentioned experiments. Again, under the same overpotential, the semi-circle's diameter corresponding the annealed sample is smaller than the non-annealed one in acidic condition, which means a smaller charge transfer resistance, thus signifying a superior HER catalytic activity [36]. This is a just the opposite case for the before- and after-durability-test samples tested in NaOH. Besides, other samples' Nyquist plots shown in Fig. S4 are also directly in accordance with their projected HER activity.

Conclusions

Ni–P nanoparticles with their size as small as 40–80 nm can be prepared via a facile and cost-effective reduction reaction. HER activity varies according to different testing conditions and samples of different heat treatment times. The 4-h-annealed sample shows the best HER activity in H_2SO_4, whereas in NaOH, it is the non-heat-treated one that performs better. The Ni–P nanoparticles' excellent HER activity can be attributable to their well dispersity, nanomaterials' small size, as well as the ensemble effect between charged nickel and phosphorus. More works still need to be done to elucidate phenomena in the experiments, especially the relations between HER activity and different nickel phosphide phases. Considering transition metal phosphides' promising prospect as the new type HER electrocatalyst in the future, it is worth paying consecutive attention to this category of materials.

Acknowledgements

This study is supported by the National Science Fund for Distinguished Young Scholars (No. 51125016),

and the National Natural Science Foundation of China (Nos. 51371119, 51571151, and 51671143).

Electronic supplementary material: The online version of this article (doi:10.1007/s10853-016-0377-7) contains supplementary material, which is available to authorized users.

References

[1] Kibsgaard J, Jaramillo TF (2014) Molybdenum Phosphosulfide: an active, acid-stable, earth-abundant catalyst for the hydrogen evolution reaction. Angew Chem Int Ed 53(52):14433–14437

[2] Laursen A, Patraju K, Whitaker M, Retuerto M, Sarkar T, Yao N, Ramanujachary K, Greenblatt M, Dismukes G (2015) Nanocrystalline Ni5P4: a hydrogen evolution electrocatalyst of exceptional efficiency in both alkaline and acidic media. Energ Environ Sci 8(3):1027–1034

[3] Walter MG, Warren EL, McKone JR, Boettcher SW, Mi Q, Santori EA, Lewis NS (2011) Correction to solar water splitting cells. Chem Rev 111(9):5815–5815

[4] Cook TR, Dogutan DK, Reece SY, Surendranath Y, Teets TS, Nocera DG (2010) Solar energy supply and storage for the legacy and nonlegacy worlds. Chem Rev 110(11):6474–6502

[5] Popczun EJ, McKone JR, Read CG, Biacchi AJ, Wiltrout AM, Lewis NS, Schaak RE (2013) Nanostructured nickel phosphide as an electrocatalyst for the hydrogen evolution reaction. J Am Chem Soc 135(25):9267–9270

[6] Chen WF, Sasaki K, Ma C, Frenkel AI, Marinkovic N, Muckerman JT, Zhu Y, Adzic RR (2012) Hydrogen-evolution catalysts based on non-noble metal nickel-molybdenum nitride nanosheets. Angew Chem Int Ed 51(25):6131–6135

[7] Liu P, Rodriguez JA (2005) Catalysts for hydrogen evolution from the [nife] hydrogenase to the ni2p(001) surface: the importance of ensemble effect. J Am Chem Soc 127(42):14871–14878

[8] Kibsgaard J, Chen Z, Reinecke BN, Jaramillo TF (2012) Engineering the surface structure of MoS2 to preferentially expose active edge sites for electrocatalysis. Nat Mater 11(11):963–969

[9] Voiry D, Salehi M, Silva R, Fujita T, Chen M, Asefa T, Shenoy VB, Eda G, Chhowalla M (2013) Conducting MoS2 nanosheets as catalysts for hydrogen evolution reaction. Nano Lett 13(12):6222–6227

[10] Han A, Jin S, Chen H, Ji H, Sun Z, Du P (2015) A robust hydrogen evolution catalyst based on crystalline nickel phosphide nanoflakes on three-dimensional graphene/nickel foam: high performance for electrocatalytic hydrogen production from pH 0–14. J Mater Chem A 3(5):1941–1946

[11] Pu Z, Liu Q, Jiang P, Asiri AM, Obaid AY, Sun X (2014) CoP nanosheet arrays supported on a Ti plate: an efficient cathode for electrochemical hydrogen evolution. Chem Mater 26(15):4326–4329

[12] Tian J, Liu Q, Cheng N, Asiri AM, Sun X (2014) Self-supported Cu3P nanowire arrays as an integrated high-performance three-dimensional cathode for generating hydrogen from water. Angew Chem Int Ed 53(36):9577–9581

[13] Jiang P, Liu Q, Liang Y, Tian J, Asiri AM, Sun X (2014) A cost-effective 3d hydrogen evolution cathode with high catalytic activity: FeP nanowire array as the active phase. Angew Chem Int Ed 53(47):12855–12859

[14] Jiaqiang G, Yating W, Lei L, Bin S, Wenbin H (2005) Crystallization temperature of amorphous electroless nickel–phosphorus alloys. Mater Lett 59(13):1665–1669

[15] Pan Y, Liu Y, Zhao J, Yang K, Liang J, Liu D, Hu W, Liu D, Liu Y, Liu C (2015) Monodispersed nickel phosphide nanocrystals with different phases: synthesis, characterization and electrocatalytic properties for hydrogen evolution. J Mater Chem A 3(4):1656–1665

[16] Wan L, Zhang J, Chen Y, Wang H, Hu W, Liu L, Deng Y (2015) Preparation, characterization and microwave absorbing properties of nano-sized yolk-in-shell Ni–P nanospheres. J Phys D Appl Phys 48(35):1–9

[17] Wang H, Wan L, Chen Y, Hu W, Liu L, Zhong C, Deng Y (2015) Fabrication and microwave absorbing properties of NixPy nanotubes. J Phys D Appl Phys 48(21):1–7

[18] Huang Z, Chen Z, Chen Z, Lv C, Meng H, Zhang C (2014) Ni12P5 nanoparticles as an efficient catalyst for hydrogen generation via electrolysis and photoelectrolysis. ACS Nano 8(8):8121–8129

[19] Deng Y, Wang H, Xu L, Wu Y, Zhong C, Hu W (2013) Autocatalytic-assembly based on self-decomposing templates: a facile approach toward hollow metal nanostructures. RSC Adv 3(14):4666–4672

[20] Wang H, Wan L, Chen Y, Hu W, Deng Y (2015) Hydrothermal synthesis, characterisation and growth mechanism of Ni (SO4) 0.3 (OH) 1.4 nanowires. IET Micro Nano Lett 10(10):567–572

[21] Randin JP, Maire P, Saurer E, Hintermann H (1967) DTA and X-ray studies of electroless nickel. J Electrochem Soc 114(5):442–445

[22] Zhang H, Lu Y, Gu C-D, Wang X-L, Tu J-P (2012) Ionothermal synthesis and lithium storage performance of core/shell structured amorphous@ crystalline Ni–P nanoparticles. CrystEngComm 14(23):7942–7950

[23] Elsener B, Atzei D, Krolikowski A, Rossi A (2008) Effect of phosphorus concentration on the electronic structure of

nanocrystalline electrodeposited Ni–P alloys: an XPS and XAES investigation. Surf Interface Anal 40(5):919–926

[24] Zhang H, Gu C-D, Huang M-L, Wang X-L, Tu J-P (2013) Anchoring three-dimensional network structured Ni–P nanowires on reduced graphene oxide and their enhanced electrocatalytic activity towards methanol oxidation. Electrochem Commun 35:108–111

[25] Zhao Y, Zhao Y, Feng H, Shen J (2011) Synthesis of nickel phosphide nano-particles in a eutectic mixture for hydrotreating reactions. J Mat Chem 21(22):8137–8145

[26] Li J, Chai Y, Liu B, Wu Y, Li X, Tang Z, Liu Y, Liu C (2014) The catalytic performance of Ni 2 P/Al 2 O 3 catalyst in comparison with Ni/Al 2 O 3 catalyst in dehydrogenation of cyclohexane. Appl Catal A 469:434–441

[27] Feng L, Vrubel H, Bensimon M, Hu X (2014) Easily-prepared dinickel phosphide (Ni 2 P) nanoparticles as an efficient and robust electrocatalyst for hydrogen evolution. Phys Chem Chem Phys 16(13):5917–5921

[28] Jin Z, Li P, Huang X, Zeng G, Jin Y, Zheng B, Xiao D (2014) Three-dimensional amorphous tungsten-doped nickel phosphide microsphere as an efficient electrocatalyst for hydrogen evolution. J Mater Chem A 2(43):18593–18599

[29] Kamat PV (2007) Meeting the clean energy demand: nanostructure architectures for solar energy conversion. J Phys Chem C 111(7):2834–2860

[30] Benck JD, Hellstern TR, Kibsgaard J, Chakthranont P, Jaramillo TF (2014) Catalyzing the hydrogen evolution reaction (HER) with molybdenum sulfide nanomaterials. ACS Catal 4(11):3957–3971

[31] Hu S, Shaner MR, Beardslee JA, Lichterman M, Brunschwig BS, Lewis NS (2014) Amorphous TiO2 coatings stabilize Si, GaAs, and GaP photoanodes for efficient water oxidation. Science 344(6187):1005–1009

[32] Cai J, Xu J, Wang J, Zhang L, Zhou H, Zhong Y, Chen D, Fan H, Shao H, Zhang J (2013) Fabrication of three-dimensional nanoporous nickel films with tunable nanoporosity and their excellent electrocatalytic activities for hydrogen evolution reaction. Int J Hydrogen Energy 38(2):934–941

[33] Ahn SH, Hwang SJ, Yoo SJ, Choi I, Kim H-J, Jang JH, Nam SW, Lim T-H, Lim T, Kim S-K (2012) Electrodeposited Ni dendrites with high activity and durability for hydrogen evolution reaction in alkaline water electrolysis. J Mat Chem 22(30):15153–15159

[34] McEnaney JM, Crompton JC, Callejas JF, Popczun EJ, Biacchi AJ, Lewis NS, Schaak RE (2014) Amorphous molybdenum phosphide nanoparticles for electrocatalytic hydrogen evolution. Chem Mater 26(16):4826–4831

[35] Wang X, Kolen'ko YV, Bao XQ, Kovnir K, Liu L (2015) One-step synthesis of self-supported nickel phosphide nanosheet array cathodes for efficient electrocatalytic hydrogen generation. Angew Chem Int Ed 54(28):8188–8192

[36] Guo CX, Zhang LY, Miao J, Zhang J, Li CM (2013) DNA-functionalized graphene to guide growth of highly active pd nanocrystals as efficient electrocatalyst for direct formic acid fuel cells. Adv Energy Mater 3(2):167–171